

dispersed genes in different lineages. First, the cluster may have been broken up in organisms with elevated rates of genome evolution, such as *C. intestinalis*, *C. elegans* and *Drosophila melanogaster*. This implies that cluster integrity in other lineages may not be due to selection. Conversely, clusters may have been maintained in some lineages due to selection. This would imply a relaxation of selection in lineages that have undergone cluster breakup. In this context it is notable that those lineages that have undergone Fox cluster breakup (*C. intestinalis*, *C. elegans* and *D. melanogaster*) also show Hox cluster breakup (Supplemental Data).

Gene expression has previously provided important insight into the nature of selective forces acting on gene clusters [1] and amphioxus has proven useful for identifying the primitive role of developmental genes [9]. Consequently, we compared the expression of *FoxL1*, *FoxC*, *FoxF* and *FoxQ1* in amphioxus embryos [10]. Our results show that all four genes are activated sequentially in the developing endo-mesoderm (Figure 1B). *FoxL1* and *FoxC* are activated in the mesoderm of the early neurula, and later come to mark different dorsal mesoderm compartments. *FoxF* is activated at the end of neurulation, and marks the ventral mesoderm. *FoxQ1* is activated later still in the developing endoderm [10].

These data highlight co-ordinated endo-mesodermal expression as a potential selective force for maintaining Fox gene clustering. This is supported by functional studies in vertebrates and *Drosophila*, in which manipulation of *FoxF*, *FoxC*, *FoxL1* and *FoxQ1* gene function has resulted in a variety of mesoderm-associated phenotypes. Importantly, a feature often observed in such manipulations is a transformation in the identity of mesoderm compartments, suggesting a role for the Fox genes in regulating compartment identity (Supplemental data).

Our data demonstrate that a small cluster of Fox genes evolved

prior to the radiation of crown bilaterians and has been at least partially maintained in several lineages, including amphioxus, vertebrates and the honeybee, for over 500 million years. Furthermore, regulation of endo-mesoderm development may be a potential selective constraint underlying Fox gene cluster maintenance. Thus, preservation of ancient gene clustering may be more widespread than previously recognised.

#### Supplemental data

Supplemental data including Experimental Procedures are available at <http://www.current-biology.com/cgi/content/full/16/9/R314/DC1/>

#### References

1. Krumlauf, R. (1994). Hox genes in vertebrate development. *Cell* 78, 191–201.
2. Brooke, N.M., Garcia-Fernandez, J., and Holland, P.W.H. (1998). The ParaHox gene cluster is an evolutionary sister of the Hox gene cluster. *Nature* 392, 920–922.
3. Luke, G.N., Castro, L.F., McLay, K., Bird, C., Coulson, A., and Holland, P.W. (2003). Dispersal of NK homeobox gene clusters in amphioxus and humans. *Proc. Natl. Acad. Sci. USA* 100, 5292–5295.
4. Nusse, R. (2001). An ancient cluster on Wnt paralogues. *Trends Genet.* 17, 443.
5. Kaestner, K.H., Knochel, W., and Martinez, D.E. (2000). Unified nomenclature for the winged helix/forkhead transcription factors. *Genes Dev.* 14, 142–146.
6. Carlsson, P., and Mahlapuu, M. (2002). Forkhead transcription factors: key players in development and metabolism. *Dev. Biol.* 250, 1–23.
7. Mazet, F., Yu, J.K., Liberles, D.A., Holland, L.Z., and Shimeld, S.M. (2003). Phylogenetic relationships of the Fox (Forkhead) gene family in the Bilateria. *Gene* 316, 79–89.
8. Magie, C.R., Pang, K., and Martindale, M.Q. (2005). Genomic inventory and expression of Sox and Fox genes in the cnidarian *Nematostella vectensis*. *Dev. Genes Evol.* 215, 618–630.
9. Holland, L.Z., Laudet, V., and Schubert, M. (2004). The chordate amphioxus: an emerging model organism for developmental biology. *Cell. Mol. Life Sci.* 61, 2290–2308.
10. Mazet, F., Luke, G.N., and Shimeld, S.M. (2005). The amphioxus *FOXQ1* gene is expressed in the developing endostyle. *Gene Expression Patterns* 5, 313–315.

<sup>1</sup>School of Biological Sciences, University of Reading, Whiteknights, Reading RG6 6AJ, UK. <sup>2</sup>Benaroya Research Institute at Virginia Mason, 1201 Ninth Avenue, Seattle WA 98101, USA. <sup>3</sup>Department of Zoology, University of Oxford, South Parks Road, Oxford OX1 3PS, UK. \*E-mail: [sebastian.shimeld@zoology.oxford.ac.uk](mailto:sebastian.shimeld@zoology.oxford.ac.uk)

## Nanosecond-scale kinetics of nematocyst discharge

Timm Nüchter<sup>1</sup>, Martin Benoit<sup>2</sup>, Ulrike Engel<sup>3,4</sup>, Suat Özbek<sup>4</sup> and Thomas W. Holstein<sup>1,3,4,5</sup>

The rapid discharge of stinging cells (nematocytes) in jellyfish, hydra, and other cnidarians is one of the fastest movements in the animal kingdom. After the triggering of exocytosis, a miniature cellular weapon, the nematocyst, is released and stylets punch a hole into the prey's integument. This step is so fast that conventional high-speed micro-cinematography fails to resolve its kinetics [1]. Here we use electronic framing-streak cameras and show kinetics of discharge to be as short as 700 ns creating an acceleration of up to 5,410,000 g. Our study identifies an ingenious solution combining vesicle exocytosis with a powerful molecular spring mechanism releasing energy stored in the mini-collagen polymer within nanoseconds.

Figure 1A shows the discharge of a stenotele nematocyst, a giant exocytotic organelle. The nematocyst capsule has a wall consisting of small disulfide-linked collagen-like molecules, called mini-collagens [2–4]. It is filled with a matrix of charged  $\gamma$ -glutamate polymers and cations [5] generating a high internal pressure (15 MPa) that drives discharge [4,5]. We mimicked the receptor potential triggering nematocyst discharge [6] by applying a short-step depolarization and analyzed discharge in >1200 instances with an electronic framing-streak camera (for details see Figure S1 in Supplemental Data). We resolved the ultra-fast phase of discharge by capturing an intermediate stage between the resting capsule and the fully ejected stylet at an exposure time of 200 ns and a framing rate of 1,430,000 fps (Figure 1B). Even at this rate we recorded sequences where this intermediate stage was lacking (Figure S2). Analysis of the discharge revealed

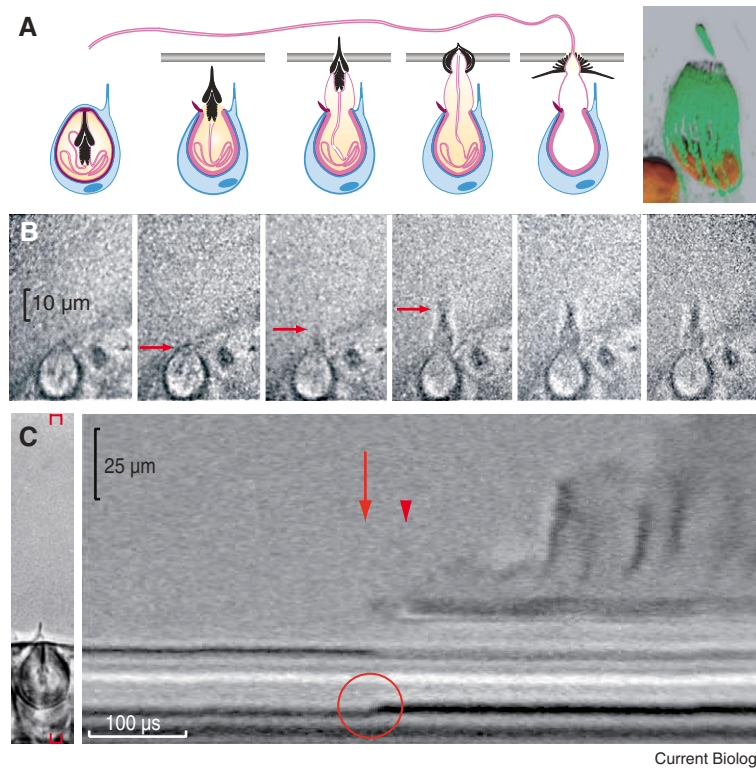


Figure 1. Discharge of a stenotele nematocyst shown schematically (A) and recorded with a Hamamatsu C4187 high-speed camera in the (B) framing and (C) streak mode. (A) Nematocytes (blue; cell and vesicle membranes in dark blue) harbor one cyst (pink; minicollagen wall, tubule, and operculum) with stylets (black) punching a hole into prey; the 2-photon micrograph inset shows microtubules anchoring the capsule (tubulin antibody, green; DAPI-stained nucleus, red). (B) Sequential images, taken 195  $\mu$ s after triggering at 1,430,000 frames per second (200 ns exposure time, 500 ns frame interval); arrows indicate progress of discharge. (C) Streak record at 3  $\mu$ s resolution: 915  $\mu$ s after triggering (i) stylets eject (arrow) followed by (ii) wall contraction (red circle), (iii) a short arrest phase (red arrowhead) and (iv) tubule eversion. Micrograph on left shows slit position (red brackets) during discharge.

that the stylet tip travels a distance (s) of 13  $\mu$ m within a time (t) of 0.7–1.4  $\mu$ s at an average velocity ( $v_{avg} = s/t$ ) of 9.3–18.6 m/s. We calculate a constant acceleration ( $a = 2 \times s/t^2$ ) from  $1.35 \times 10^6$  g up to  $5.41 \times 10^6$  g ( $g = 9.81$  m/sec<sup>2</sup>), which is two orders of magnitude greater than previous measurements [1].

This acceleration generates sufficient impact to penetrate the cuticle of crustacean prey, even though the accelerated mass is very small. Assuming constant acceleration, we calculate that the stylets hit the cuticle with a final velocity ( $v_{max} = a \times t$ ) of 18.5–37.1 m/s. At an average volume (V) of 1860  $\mu$ m<sup>3</sup> and a specific density ( $\rho$ ) of  $1.24 \times 10^6$  kg/m<sup>3</sup> [7], the stenotele's mass ( $m = \rho \times V$ ) is 2.3 ng. Since 40% of this mass gets ejected along with the stylets, the accelerated mass is about 1 ng. This corresponds to an accelerating

force ( $F = m \times a$ ) of 13.2–53.1  $\mu$ N and a kinetic energy ( $E = 1/2 \times m \times v_{max}^2$ ) of 0.17–0.7  $\mu$ J. Due to the extremely narrow tip of stylets (tip radius  $15 \pm 8$  nm), the pressure ( $F/\text{area}$ ) at a stylet's tip can be estimated to be more than 7 GPa, which is in the range of technical bullets.

The streak mode of the camera displayed a 'smear' picture of discharge revealing two steps with very different kinetics (Figure 1C). In the first, exceedingly fast step, the stylet apparatus is ejected from the capsule; in a second slower process the stylets open out and the tubule is everted through itself. Stylet ejection was mostly visible as an abrupt, step-like dislocation without any previous changes in the capsule; in less than 20% of all records were changes in capsules observed prior to stylet ejection (Figure S3). After stylet ejection, the capsule contracted to 70%

( $18 \pm 6$   $\mu$ s) and, following an arrest phase, to 50% of the original volume [1] (also see Supplemental Results and Discussion). Tubule eversion ( $2.7 \pm 0.21$  m/s) was accompanied by 50  $\mu$ s periodicities along the trace of the everting tubule, probably due to rotary movements of the tubule or to contractions of the collagen wall. During the entire discharge process the capsule did not change its position inside the cell, indicating that the organelle is efficiently anchored by microtubules (Figure 1A).

When we analyzed the delay phase between stimulation and stylet ejection (exocytosis), this phase proved to be highly dependent on extracellular  $\text{Ca}^{2+}$  (Figure 2). At 1 mM  $\text{Ca}^{2+}$  (culture medium) delay times varied from 300 to 1200  $\mu$ s with an average delay of  $650 \pm 134$   $\mu$ s. Lowering the  $\text{Ca}^{2+}$  concentration postponed discharge to >1 ms and depletion of calcium (EDTA) completely inhibited the discharge process. Increasing the  $\text{Ca}^{2+}$  concentration shortened the delay and minimal delay times (~200  $\mu$ s) were in the range of fast synaptic vesicles [8].

The osmotically active polymeric ion-exchange matrix, which drives discharge of nematocysts, is a feature shared by other exocytotic organelles, e.g. chromaffin granules in chromaffin cells [9]. The unique feature of *Hydra* nematocysts is that they are under a high initial osmotic pressure prior to discharge [1,10], which stretches the capsule

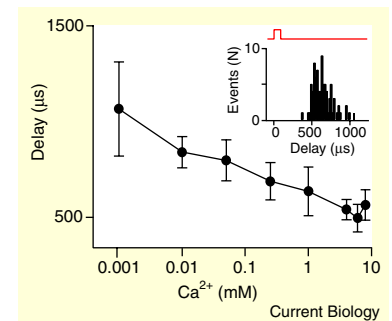


Figure 2.  $\text{Ca}^{2+}$  dependency of discharge. The length of delay times between membrane depolarization and stylet ejection (exocytosis) were measured with the streak camera (Figure 1B), and mean values (linear scale) are plotted against  $\text{Ca}^{2+}$  concentration (log scale); bars indicate SD. Inset shows a distribution of delay times at 1 mM  $\text{Ca}^{2+}$  and the voltage (red).

wall. We propose that the high speed of discharge is due to the release of energy stored in the stretched configuration of the collagen polymer of the capsule wall. How the ejection of the stylets is initiated during exocytosis and after fusion pore formation remains to be shown.

#### Acknowledgements

This work was supported by the DFG and Hamamatsu Photonics Germany. We thank Uwe Denzer for his generous help.

#### Supplemental data

Supplemental data including Experimental Procedures are available at <http://www.current-biology.com/cgi/content/full/16/9/R316/DC1/>

#### References

- Holstein, T., and Tardent, P. (1984). An ultrahigh-speed analysis of exocytosis: nematocyst discharge. *Science* 223, 830–833.
- Kurz, E.M., Holstein, T.W., Petri, B.M., Engel, J., and David, C.N. (1991). Mini-collagens in hydra nematocytes. *J. Cell Biol.* 115, 1159–1169.
- Engel, U., Pertz, O., Fauser, C., Engel, J., David, C.N., and Holstein, T.W. (2001). A switch in disulfide linkage during minicollagen assembly in Hydra nematocysts. *EMBO J.* 20, 3063–3073.
- Holstein, T.W., Benoit, M., Herder, G.V., Wanner, G., David, C.N., and Gaub, H.E. (1994). Fibrous mini-collagens in Hydra nematocysts. *Science* 265, 402–404.
- Weber, J. (1989). Nematocysts (stinging capsules of Cnidaria) as Donnan-potential dominated osmotic systems. *J. Biol. Chem.* 265, 9664–9669.
- Brinkmann, M., Oliver, D., and Thurm, U. (1996). Mechanoelectric transduction in nematocytes of a hydrozoan (Corynidae). *J. Comp. Physiol.* 178A, 125–138.
- Weber, J., Klug, M., and Tardent, P. (1987). Some physical and chemical properties of purified nematocysts of *Hydra attenuata* Pall. (Hydrozoa, Cnidaria). *Comp. Biochem. Physiol.* 88B, 855–862.
- Fix, M., Melia, T.J., Jaiswal, J.K., Rappoport, J.Z., You, D., Sollner, T.H., Rothman, J.E., and Simon, S.M. (2004). Imaging single membrane fusion events mediated by SNARE proteins. *Proc. Natl. Acad. Sci. USA* 101, 7311–7316.
- Fernandez, J.M., Villalon, M., and Verdugo, P. (1991). Reversible condensation of mast cell secretory products in vitro. *Biophys. J.* 59, 1022–1027.
- Szczepanek, S., Cikala, M., and David, C.N. (2002). Poly-gamma-glutamate synthesis during formation of nematocyst capsules in *Hydra*. *J. Cell Sci.* 115, 745–751.

<sup>1</sup>Institute of Zoology, University of Frankfurt, Theodor-Stern-Kai 7, 60590 Frankfurt am Main, Germany.

<sup>2</sup>Department for Applied Physics, LM University Munich, 80799 München, Germany.

<sup>3</sup>Department of Biology, Darmstadt University of Technology, Schnittpahnstrasse 10, 64287 Darmstadt, Germany.

<sup>4</sup>Heidelberg Institute of Zoology, University of Heidelberg, 69120 Heidelberg, Germany.

<sup>5</sup>E-mail: [holstein@uni-hd.de](mailto:holstein@uni-hd.de)

## Molecular evidence for dim-light vision in the last common ancestor of the vertebrates

Davide Pisani<sup>1,2\*</sup>,  
Samantha M. Mohun<sup>2</sup>,  
Simon R. Harris<sup>3</sup>,  
James O. McInerney<sup>1</sup>  
and Mark Wilkinson<sup>2</sup>

Animal vision is mediated through pigments belonging exclusively to the opsin family. These are members of the G-protein-coupled receptor family that bind retinal [1]. Based on function and phylogenetic relationship, vertebrate visual opsins can be clustered in five groups: Rhod photoreceptors (Rh1), Rh1-like (Rh2), Short Wave Sensitive (SWS1), SWS1-like (SWS2), and Long (LWS) or Medium (MWS) Wave Length Sensitive (LWS/MWS). Rh1 is used for seeing under dim light conditions (scotopic vision), while the others permit full colour (photopic) vision in bright light [2–5]. Opsins have diversified by a series of gene duplications, and the inferred

order of these duplications indicates that photopic vision predated scotopic vision in vertebrates [2–5].

Assuming that the jawless vertebrates (Agnatha) are monophyletic [6], the broad distribution of opsins associated with photopic vision indicates that these – and thus the capacity for photopic vision – were present in the last common ancestor of all living vertebrates [2–5]. However, it is still unclear whether ‘true’ (i.e., Rh1-mediated [3]) dim-light vision predated the split between Agnatha and the jawed vertebrates (Gnathostomata), or whether it is an apomorphy of the Gnathostomata [2–5,7]. Solving this question has important palaeoecological implications and, assuming that orthologous opsins have inherited a common ancestral function, it depends on the correct classification (phylogeny based orthologous clustering) of the few agnathan Rh sequences available to date.

Based on a Neighbour Joining (NJ) analysis, Yokoyama [2] suggested that the two agnathan Rh sequences available at that time represented Rh1 opsins. This would imply that the vertebrate ancestor was potentially capable of

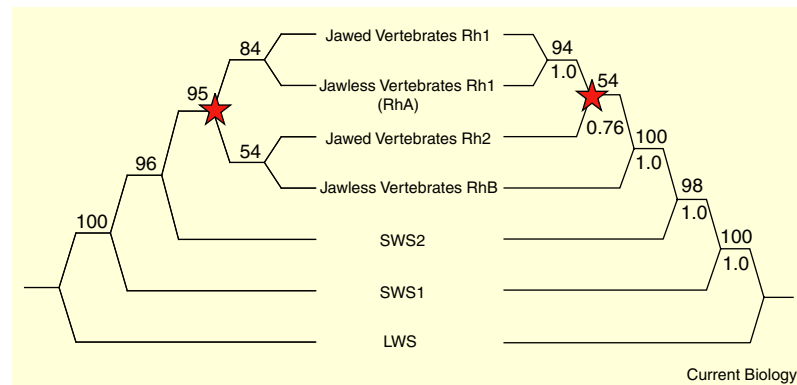


Figure 1. Phylogenetic relationships among vertebrate visual opsins.

The left tree shows a summary of the relationships obtained from the quartet puzzling and the minimum evolution analyses (Supplemental data). Numbers at the nodes represent quartet-puzzling support values. The right tree shows a summary of the relationships obtained in the ML analyses (PHYML, SPR-PHYML and SPR), in the Bayesian analysis, and in the equally and differentially weighted parsimony analyses (Supplemental data). Numbers at the nodes represent the bootstrap support values obtained in the PHYML analysis (above) and posterior probabilities (below). The red star represents the gene duplication resulting in the origin of Rh1.